Experimental and analytical investigation of a highly integrated electro-hydraulic pump motor unit

Lukas Matias[12], Andrew Plummer[1], and Nigel Johnston[1]

[1] Centre for Power Transmission and Motion Control, University of Bath, UK
[2] Domin Limited, Bristol, UK
Email: lwnm20@bath.ac.uk; lukas.matias@domin.com

Abstract

Hydraulic pumps driven by electric motors (ePumps) sit at the core of the electrification of hydraulic systems with applications in electro-hydrostatic actuation for aerospace, automotive and construction machinery. ePumps are rarely designed as an integrated unit, but use readily available pumps and electric motors, coupled via a drive shaft. Aerospace and automotive applications require high power density and compactness to minimize space and weight requirements on the vehicle. This paper presents the experimental and analytical investigation of a novel design integrating a radial piston pump and brushless DC motor into a single very compact unit. ePump volumetric and mechanical losses are investigated experimentally, and analytical modelling approaches are used to assess pump loss results. Methods for testing and modelling are integrated into a framework, outlining a comprehensive approach for the investigation of losses within ePumps. The breakdown of measured losses for such a unit presents a challenge however, as the pump shaft is not easily accessible in order to measure torque. One approach is to infer frictional losses in the pump by experimentally determining overall power loss and subtracting volumetric pump loss. Overall power loss is the difference between electrical input power and fluid output power, and so in this approach the electric machine and power electronics losses are not accounted for. To separate electrical machine losses from frictional losses in the pump, a measurement of the pump shaft torque is required. A non-invasive method of measuring the drive shaft torque via the reaction torque on the motor stator is proposed and was successfully proven out. The torque results have yielded credible and repeatable results, enabling the analysis of power loss fractions. The comparison between analytical and experimental results allowed to identify medium speeds and higher pressures as favourable operating conditions of the unit, as per design intent. The successfully validated ePump loss analysis framework will provide a guide for a detailed breakdown of losses in highly integrated electric pumps, facilitating improved designs with high energy-efficiency and a high level of compactness.

Keywords: ePump, integrated electro-hydraulic pump motor, radial piston pump, brushless DC motor, electrification

1 Introduction

Highly integrated ePumps are a key enabler in the electrification of hydraulic systems. Applications range from off-highway vehicles [1] [2] to automotive brake-by-wire (BBW) systems [3] and aerospace actuation [4]. The electrification of hydraulic systems has become a key research area to facilitate the transition towards low carbon emissions from the transport sector as part of initiatives such as the European Green Deal [5], calling for a 90% reduction in transport emissions by 2050. Fixed displacement pumps coupled with variable speed drives are the most common drive configuration for decentralized electro-hydraulic actuators [6], enabling more energy-efficient hydraulic systems. Typically, the electric motor and pump are separate components, and the integrated design can offer the benefits of a reduced package size, a lightweight design and the opportunity to coordinate the design of pump and motor for optimized performance.

A commercial design was first presented by Voith Turbo, integrating an internal gear unit within an asynchronous electric motor and promoting low noise emissions as well as up to 50% less space requirements compared to conventional solutions [7]. Today, the system is not available anymore. In 2007, Wustmann and Helduser first introduced a design concept for an external gear pump centrally integrated within

a switched reluctance motor to enable a higher level of integration over the common shaft coupling [8]. The design eliminated shaft seals and offered the opportunity of electric motor cooling to enhance thermal durability. However, in simulation the design only proved feasible for low pressure applications and featured a large amount of unused structural space. The external gear pump based concept was picked up again by Zappaterra et al. in 2022 [9]. An optimization study considering both pump and electric motor parameters was presented, and a prototype experimentally validated.

A gerotor pump based design, with the outer gear acting as the electric motor rotor and directly driven by the motor was presented in 2017 by Gamez-Montero et al. [10]. The feasibility of the design was experimentally proven with limitations in pump speed (test only up to 500 rpm), but expected benefits in noise.

In a similar approach, Fiebig et al. presented a vane pump based design [11] in 2014. The vane pump sits in the centre of a surrounding brushless direct-current (BLDC) motor, achieving a 40% reduction in volume compared to conventional designs, according to the authors. The analysis work centred on proving the dynamic control benefits of such a system. In 2017 and 2021, the research group followed up with an experimental proof-of-concept of the vane pump design, validating its control performance and the ability to build pressure and deliver flow [12] and [13].

An axial piston machine concept was first published by Wang and Zhou [14] in 2016. Following an analysis of preferable integration structures, the pump-in-centre approach was again adapted with the cylinder barrel acting as the electric rotor and directly driven by the motor. A first experimental proof-of-concept was successful. A similar design approach was taken by Zhu et al. in 2020, with the focus on an aerospace application [15]. Sarode et. al. presented a permanent magnet synchronous motor (PMSM) drive axial piston machine for off-highway applications in 2023 [16]. The numerical work included the optimization of the electric motor for a set of design specification and considered typical design trade-offs in electric motors such as current density and weight.

A radial piston-based design (“TwinTorq motor”) was patented by KersTech, Inc. and combines a multi-lobed, inside-impinged hydraulic motor with an electric ring motor around the pump circumference for electric vehicle applications [17]. KersTech, Inc. promotes a high efficiency motor with 25% to 45% efficiency improvements shown in simulation over conventional units. In 2019, Bohach et al. investigated the suitability of a radial ball piston pump design in a numerical study [18]. The same research group published an analysis of suitable system topologies with a focus on the electric machine design, eventually proposing an axial flux PMSM [19]. The design of this machine was discussed in [20]. In academia, a radial piston pump design concept tightly integrated with an axial flux PMSM was presented by Nishanth et al. [21] in 2022, with the cam and cylinder block sitting inside the stator. A numerical model of the pump was discussed by Nahin et al. in [22]. Li et al. numerically studied a similar design in 2019 [23].

Most of the discussed designs are targeted at off-highway applications and are generally designed for high power applications with power ratings > 5 kW. This paper presents a novel highly integrated, additively manufactured (AM) radial piston pump unit, driven by a BLDC motor for low power automotive and aerospace applications. As discussed in [24], the application of AM technologies provides the opportunity for further improved power density, and integrated sensing and control within the unit to enable robust control and health monitoring. The presented unit not only integrates motor and pump but also features onboard power electronics and closed-loop speed control of the pump with the opportunity of sensing the motor temperature for condition monitoring.

A common challenge with highly integrated electric pumps is the breakdown of losses in the unit as part of a performance characterization. This is key in the understanding of critical design parameters. As most of the presented design solutions are shaftless, a direct pump shaft torque measurement is not possible. Whilst mechanical losses in the unit may be inferred from volumetric and total unit losses, a clear separation cannot be made. This study presents an ePump loss analysis framework, including a non-invasive torque measurement approach, to further increase the understanding of highly integrated electric pumps. This will enable improved designs for future iterations and facilitate a design process with the aim of an optimized design in terms of size, weight and efficiency.

The paper outlines the design of the prototype demonstrator unit for the purpose of this study. That is followed up with an introduction of the process and methods used for the characterization of highly integrated ePumps. The test set-up and procedure are described in detail with the addition of a pump torque test add on. An analytical model is introduced and validated against experimental data. The loss distribution within the pump is discussed and favourable operating conditions for each of the components are identified.

2 Highly integrated pump-motor unit

As a demonstrator for this study, an early prototype was used, with key specifications listed in Table 1. The ePump is designed as a fixed displacement, inside-impinged radial piston pump, directly integrated into a brushless DC motor as the primary driver. The chosen motor type is beneficial for this type of application as it is a simple design, allows for high performance speed control, and offers higher power densities. The radial piston pump architecture is favorable, as it allows a compact axial integration with the motor. The unit diameter is mainly driven by the motor, with the pump adding simply some stack length. The cam profile can be chosen freely to realize a single, or multilobed profile, allowing the the number of piston strokes per revolution to be changed. The unit uses a proven arrangement of the rotor in oil and the stator in air. They are separated by a non-magnetic pressure tube, removing the need for dynamic rotary seals. This comes at the downside of having an increased non-magnetic “airgap”, reducing the magnetic loading of the motor. Directly on top of the stator sits a printed circuit board, integrating motor driver, control and power electronics. The motor driver uses field-oriented control to achieve position (angle) and speed control of the rotor, allowing for high precision and dynamic control. The pump

and motor share a common rotor, reducing bearings and enabling an ultra-compact assembly. A schematic of the unit is shown in Figure 1. The pump features 7 pistons and a double lobed cam. This ensures a smooth operation by 14 piston strokes per revolution, minimizing flow ripple. The pump inlet is part of the AM pintle, designed to achieve a low flow resistance to minimize the risk of cavitation.

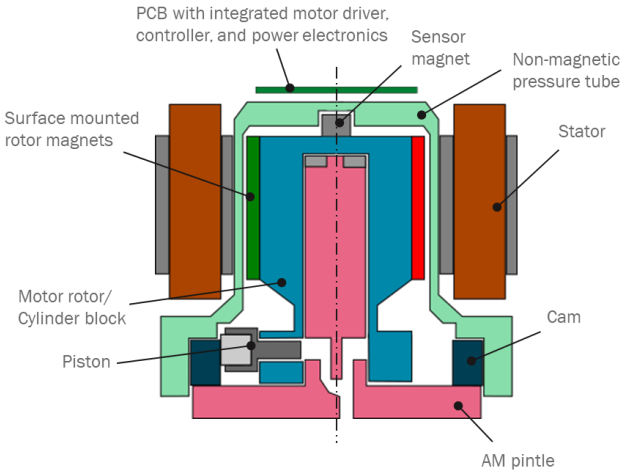

Figure 1: ePump CAD cross-section.

The key loss sources in the unit can be separated into volumetric losses and mechanical losses. Volumetric losses occur mainly as leakage between piston and piston bores, as well as between the pintle and cylinder block interface. Mechanical losses appear mainly as viscous friction in those same interfaces. Additionally, the positive force balance at the individual pistons exerts an outwards force towards the cam profile. The friction between the needle roller bearing sitting at the top of the piston and the cam results in frictional torque, opposing the rotation of the pump shaft. Furthermore, bearing friction between the interfaces of cylinder block and pressure tube as well as cylinder block and pintle is present. Lastly, churning losses occur in the flooded rotor cavity.

Table 1: ePump specifications.

Specification	**Value**
Displacement	0.55 cc/rev
Peak installed motor power	1.2 kW
Supply voltage	48 V

2.1 General method

Typically, steady-state hydraulic pump performance is evaluated based on steady state machine testing as outlined in ISO 4409:2019 [25]. Whilst discussions are ongoing on the suitability of methods outlined in the standard [26] [27], for the purpose of this work, the accepted standard will be used in the following. These tests will produce information about volumetric and mechanical losses, the effective outlet flow rate and effective inlet mechanical power for a range of operating conditions (pressure and flow). Based on those, statements about leakage and friction in the unit can be made. This understanding then feeds back into the design process where critical design parameters such as clearances, sealing land lengths, cam profile and spring rates are being defined.

Volumetric losses are considered as flow loss and are defined as the difference between the theoretical flow rate Q_{th} and the measured pump outlet flow rate Q_P:

$$Q_L = Q_{th} - Q_P \tag{1}$$

The theoretical flow rate is defined as the product of measured pump speed ω and effective pump displacement V_D:

$$Q_{th} = \omega V_D \tag{2}$$

The effective pump displacement was determined experimentally, following the approach as suggested in ISO 8426 [28]. The volumetric power loss can then be quantified to

$$P_{L,vol} = Q_L \Delta p \tag{3}$$

Mechanical loss is considered as additional pump shaft torque and is defined as the difference between the pump shaft torque (measured) T_P and the theoretical torque T_{th} that is dependent on the pressure difference across the pump Δp and the effective pump displacement:

$$T_L = T_P - T_{th} \tag{4}$$

With

$$T_{th} = \Delta p V_D \tag{5}$$

The mechanical power loss is therefore:

$$P_{L,mech} = \omega T_L \tag{6}$$

The overall power loss of the unit can be determined via the total electrical input power (measured) $P_{in,el} = I_{DCBus} V_{DCBus}$ and total hydraulic output power (measured) $P_{out,hyd} = Q_P \Delta p$ as

$$P_L = P_{in,el} - P_{out,hyd} \tag{7}$$

This finally allows the losses introduced by the electric motor and power electronics stage to be determined as the difference in losses between the combined ePump and pump:

$$P_{L,el} = P_L - (P_{L,vol} + P_{L,mech}) \tag{8}$$

As stated above, to quantify total and mechanical losses, information about the pump shaft torque is required. Due to the shaftless design, the pump cylinder block and the motor rotor are a single part (which is running in oil), and access to the rotor for mounting of an inline torque transducer is not possible. There is the option to infer electric motor torque which is assumed to be equivalent to the pump shaft torque from multiplying the measured quadrature axis current I_Q with the motor torque constant K_T:

$$T_{current} = I_Q K_T \tag{9}$$

There are however severe disadvantages of this approach. Firstly, the torque constant is often derived via simulation and

cannot be easily experimentally validated. Secondly, this approach does not allow electrical and mechanical losses to be distinguished. Previous tests have shown that motor calibration procedures heavily influence how much current is drawn for a given load on the pump. As a result, this method is not seen as appropriate for a detailed ePump performance characterization. As an alternative, a non-invasive approach to measure torque is proposed, described in Section 2.2.

With information about the pump torque $T_P = T_{EM}$ (equal to the electric motor torque), pump speed $\omega_P = \omega_{EM} = \omega$ (equal to the electric motor speed), DC bus supply current I_{DCBus} and supply voltage V_{DCBus}, electric motor and power stage losses can be stated as follows:

$$P_{L,el} = (I_{DCBus} V_{DCBus}) - (T_{EM} \omega_{EM}) \qquad (10)$$

If the operating envelope is defined according to the motor power limit envelope, this will give a very clear picture of electric motor performance in the region of interest for the ePump application. Figure 2 illustrates the proposed framework.

The results from the experimental tests will then allow pump and motor models to be validated. These models will serve as design tools for subsequent design iterations.

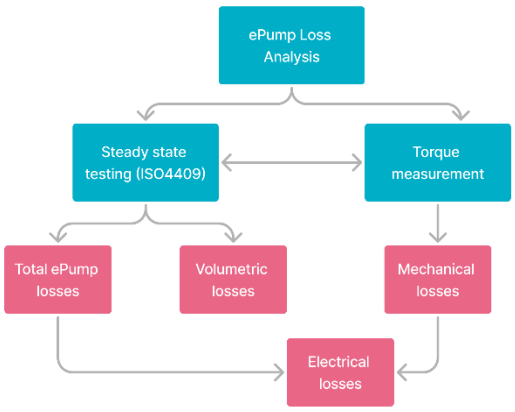

Figure 2: ePump loss analysis framework.

2.2 Non-invasive torque measurement method

Directly measuring torque in a highly integrated ePump is challenging. In this design, the motor rotor/ pump cylinder block runs in oil and is separated from the stator and power electronics via a pressure tube made from non-magnetic material. Direct access to the rotor for an inline torque sensor would require considerable changes to the design and a dynamic seal for a feed-through shaft, potentially compromising results.

As an alternative, it is proposed to measure the reaction torque on the stator via a load cell arrangement. Figure 3 shows a schematic of the set-up. The stator inner diameter sits on the pressure tube outer diameter with sufficient clearance to move freely. A mounting bracket connects to the stator and then via a rod assembly to a load cell. Ball joints on both sides of the rod ensure the elimination of side forces, that could compromise the measured force. The reaction torque leads to a force F_{LC} into the load cell, the torque $T_{reaction} = F_{LC} l$ is then determined with the known lever arm l.

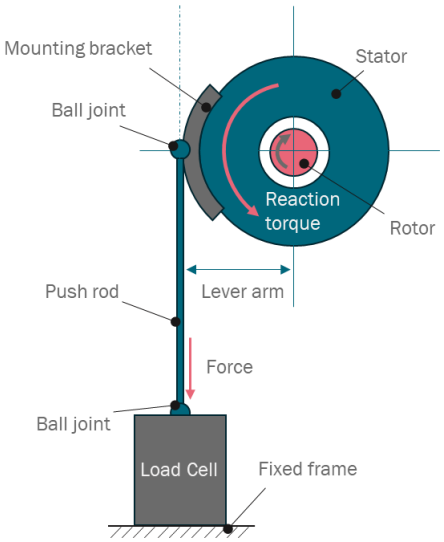

Figure 3: Schematic drawing of the load cell set-up.

2.3 Analytical loss model

For an initial analysis of the pump performance trends, a simple analytical model (constant coefficients) based on the work of Wilson, McCandlish and Dorey [29] [30] is used. The delivery flow rate of the pump is calculated as

$$Q = \omega V_D - c_s \frac{V_D \Delta p}{\mu} - \frac{\omega V_D \Delta p}{B}(V_r + 1) - c_\omega \omega \qquad (11)$$

The first term is the ideal pump flow rate. The second term represents laminar leakage flow with the slip coefficient c_s. The third term considers compressibility losses with the ratio of dead volume V_{dead} and displacement volume V_D as $V_r = V_{dead}/V_D$ and B as the bulk modulus. The fourth term is an addition to account for a speed dependence of flow losses (with c_ω as the speed coefficient) as observed in experiments and is not found in the original model descriptions.

The shaft torque is calculated as

$$T = \Delta p V_D + c_v \omega \mu V_D + c_f \Delta p V_D + T_c \qquad (12)$$

The first term is the ideal torque, and the second term considers viscous friction in the unit with the viscous friction coefficient c_v. The third term represents coulomb friction, scaled by the coulomb friction coefficient c_f. The fourth term is a constant torque component T_c and appeared in Wilsons model but was omitted in the McCandlish and Dorey models due to its usually small magnitude. It was found helpful for this analysis and is therefore included in the model.

3 Experimental validation

3.1 Power loss test set-up

The tests were conducted on a pump performance test rig, following the suggested layout as per ISO 4409 [25] and shown in Figure 4. The pump inlet is fed by a hydraulic power unit (HPU), with a pressure reducing valve allowing to set the pump inlet pressure. Tests are conducted in open circuit, with the pump outlet pressure being manually set by the pressure relief valve for each test run. The ePump speed is set via the internal pump controller. The set-up compromises flow meters, pressure transducers and temperature sensors for both inlet and outlet. The case is permanently connected to the tank line. As both inlet and outlet flow measurements are available, the drain flow is not recorded. The shaft torque is measured indirectly via the proposed load cell set-up (see Section 3.2). The motor speed is measured via a hall effect sensor, integrated into the ePump assembly. Specifications of the installed instrumentation are summarized in Table 2.

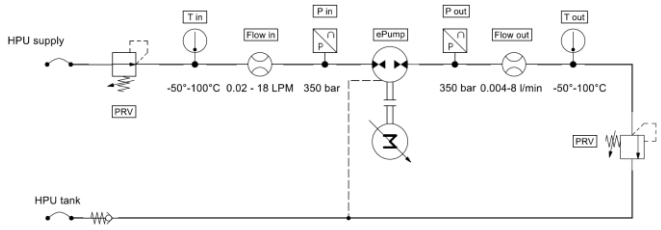

Figure 4: Pump test rig hydraulic circuit diagram.

For steady-state testing, the outlet pressure is set so that the following data points for differential pressure across the pump are generated: [22, 48, 70, 97, 122, 148, 174] bar. The outlet pressure deviation is less than 1% for each speed setting. The inlet pressure is set to approximately 7 bar. For each pressure setting, the pump speed command is varied between 25 rad/s and 175 rad/s in 25 rad/s steps. Each pressure and speed combination is held for about 25 s.

Table 2: Instrumentation.

Sensor	Model
Flow meter (inlet)	VSE Flow VS 0.2 Circular Gear Flowmeter, 0.02 – 18 LPM
Flow meter (outlet)	KOBOLD DZR-4 Gear Flowmeter 0.004 – 8 LPM
Pressure transducer (inlet)	TE Connectivity EB100 350 bar 120 Hz Bandwidth (-3dB)
Pressure transducer (outlet)	TE Connectivity EB100 350 bar 120 Hz Bandwidth (-3dB)
Temperature sensor (inlet)	RS PRO PT100 RTD 3 wire sensor -50 C to +200 C
Temperature sensor (outlet)	RS PRO PT100 RTD 3 wire sensor -50 C to +200 C
Load cell	Tedea Huntleigh Model 614 (50 kg range)

3.2 Torque measurement

To measure the torque, the anti-rotation feature keeping the stator in place during normal operation is removed and substituted by a 3D printed bracket connected to the load cell via a pushrod (Figure 5).

To validate the non-invasive torque testing method, staircase pressure ramps with quasi-steady state conditions for each step are used. For a fixed pump inlet pressure and speed, the outlet pressure is varied so that the following data points for differential pressures across the pump are generated: [4, 28, 54, 78, 103, 128, 153, 128, 103, 78, 54, 28, 4] bar. Tested pump speeds are 50, 100 and 150 rad/s. Each pressure step is held for approximately 25 s.

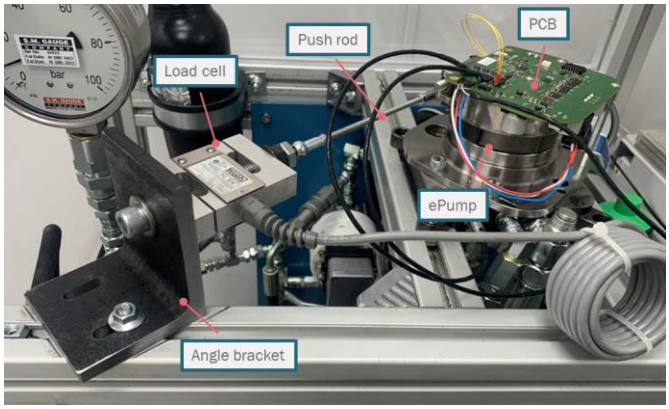

Figure 5: Image of the load cell set-up.

4 Results and discussion

4.1 Torque measurement results

Figure 6 and Figure 7 show the relationship between measured and normalized torque and pump pressure difference for 50 rad/s and 150 rad/s pump speed respectively. For commercial reasons, the torque data is normalized with respect to the maximum measured torque value for each pump speed. The results show the expected linear relationship between pump torque and differential pressure across the pump. A hysteresis effect can be observed between going up the pressure ramp and coming back down again, more distinct for 150 rad/s. The torque is lower on the downwards part of the ramp.

The hysteresis effect was further investigated and compared to the calculated torque based on the simulated torque constant and measured q-axis motor current. The deviation of the "downwards" torque with respect to the torque on the

"upwards" part of the ramp seems to grow with pump speed and is inversely proportional to the load. The motor current based torque shows a very similar trend although more distinctive and with higher magnitude (approximately double percentage deviation) in the torque results. The staircase pressure ramp tests start at 4 bar differential pressure, going up to 153 bar differential pressure and back down, with an oil temperature increase on the rig within approximately +1°C. The temperature profile within the pump is likely to be significantly different, with oil in the key clearances likely to be warmer at the end of the test, leading to lower viscosity and therefore lower torque, which is an effect that would be stronger at higher speeds.

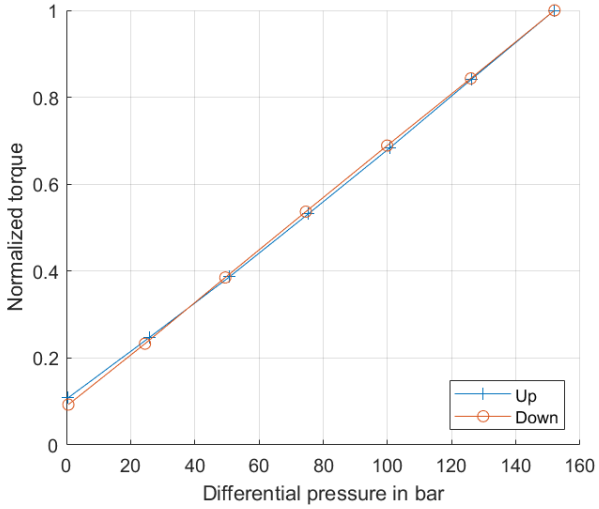

Figure 6: Torque – differential pressure relationship for 50 rad/s.

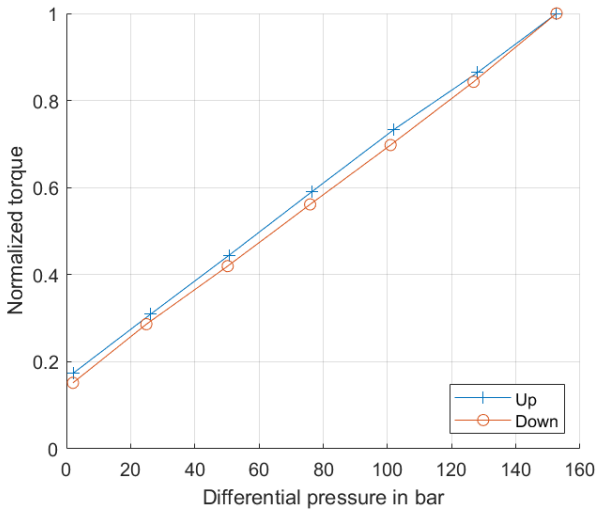

Figure 7: Torque – differential pressure relationship for 150 rad/s.

For comparison of different speeds and against the theoretical pump torque, a linear fit is applied. Figure 8 shows the results. As expected, the absolute torque for a given pressure difference is higher for higher speeds. This is due to a significant portion of the friction in the pump being viscous friction and therefore speed dependent.

It was suspected that friction between the stator inner diameter and pressure tube outer diameter might affect the measurements. The linearity and low hysteresis of the torque results, as well as the high similarity of the gradient in the measured torque vs. ideal torque in Figure 8 show that the impact of friction is not significant. The torque measurement method has yielded repeatable and creditable results.

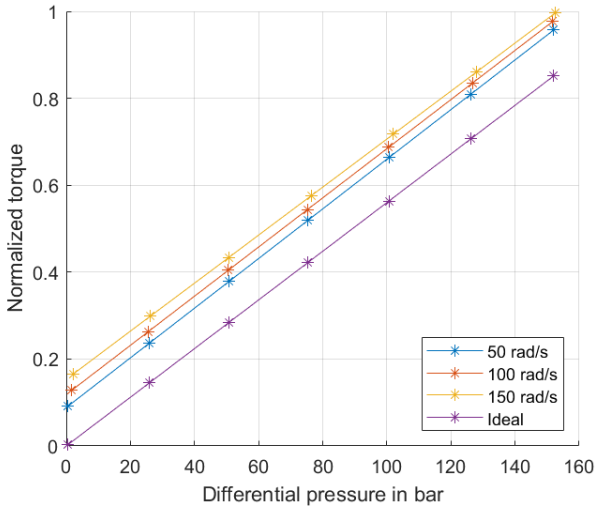

Figure 8: Torque – differential pressure relationship for a set of pump speeds.

4.2 Unit level loss results

The individual pump loss components are expressed as fractions of the total pump power loss in the following equations. The volumetric power loss fraction therefore becomes:

$$P_{L,vol,pump} = \frac{P_{L,vol}}{P_{L,vol} + P_{L,mech}} \tag{13}$$

The mechanical power loss fraction is then expressed as:

$$P_{L,mech,pump} = \frac{P_{L,mech}}{P_{L,vol} + P_{L,mech}} \tag{14}$$

Figure 9 shows the volumetric power loss fraction for three distinct pressure levels. The experimental data points are marked on the figure with an additional best fit curve to indicate trends. As expected, volumetric losses increase with higher differential pressures across the pump, due to increased leakage flow. With increasing speed, the proportion of leakage losses to outlet flow decreases. In combination with increasing viscous friction losses, the volumetric loss fraction is decreasing with increasing speed. For low pump speeds and high pump pressures, the volumetric loss is therefore the dominant loss component in the pump. The mechanical loss fraction (see Figure 10) shows the inverse pressure and speed

dependencies. The mechanical loss fraction decreases with increasing pressure. Higher pressures increase the outlet power whilst increases in friction due to pressure are much less in comparison, therefore making flow losses more distinct. As expected, the mechanical loss fraction increases with speed because of higher viscous friction and increased load on the piston bearing against the cam in the pump. For low differential pressures and high speeds, the mechanical loss is the dominant loss term in the pump.

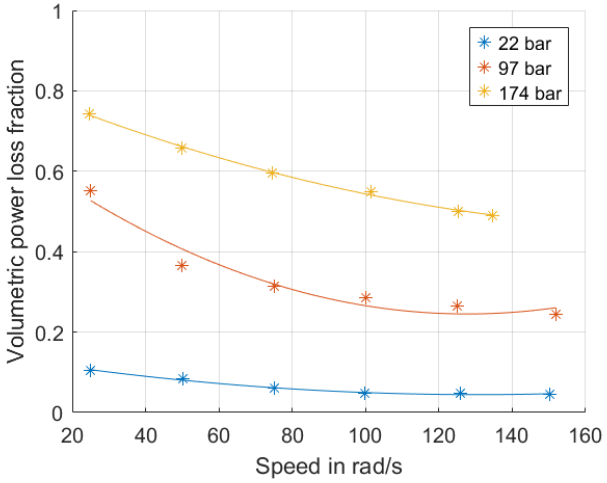

Figure 9: Volumetric loss as a fraction of pump power loss.

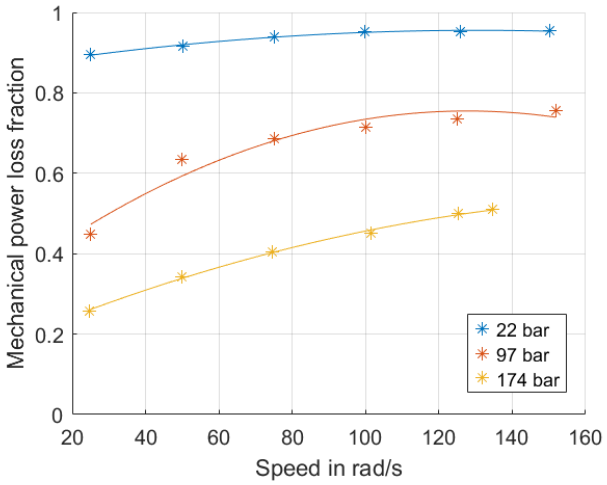

Figure 10: Mechanical loss as a fraction of pump power loss.

To facilitate understanding of loss mechanisms at a unit level, volumetric, mechanical and electrical losses are related to the total unit level losses. The volumetric loss fraction at a unit level is defined as

$$P_{L,vol,unit} = \frac{P_{L,vol}}{P_{L,el} + P_{L,vol} + P_{L.mech}} \quad (15)$$

The mechanical loss fraction at a unit level is then expressed as

$$P_{L,mech,unit} = \frac{P_{L,mech}}{P_{L,el} + P_{L,vol} + P_{L.mech}} \quad (16)$$

And the electrical loss fraction at a unit level finally becomes

$$P_{L,el,unit} = \frac{P_{L,el}}{P_{L,el} + P_{L,vol} + P_{L.mech}} \quad (17)$$

Figure 11 and Figure 12 show the contributions of the separate loss components (volumetric, mechanical, and electrical) to total unit level losses for a differential pressure of 70 bar and 148 bar respectively. The experimental data points are marked on the figure with an additional best fit curve to indicate trends.

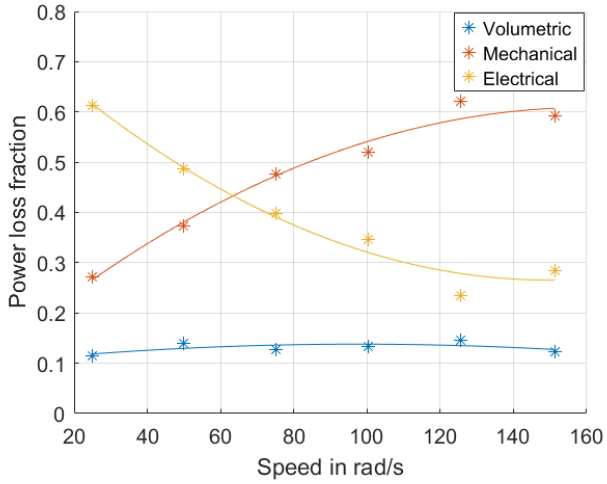

Figure 11: Volumetric, mechanical and electrical power loss as a fraction of total unit loss at 70 bar differential pressure.

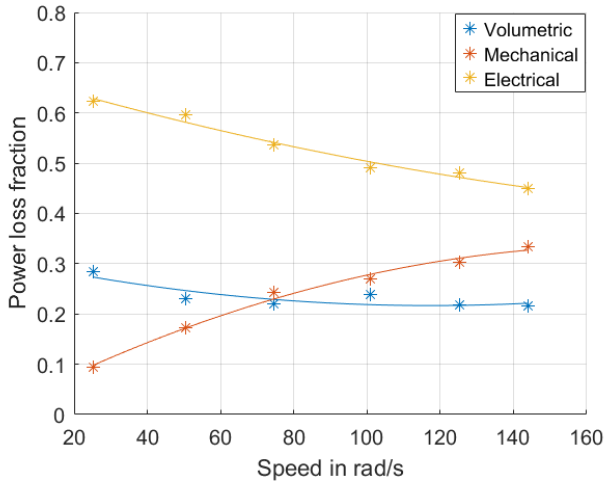

Figure 12: Volumetric, mechanical and electrical power loss as a fraction of total unit loss at 148 bar differential pressure.

For 70 bar differential pressure, the volumetric loss fraction remains near constant at an average of 14%. This is because the speed dependency of the flow loss is low and less distinct at lower pressures. The mechanical loss exhibits a clear speed dependency, with a higher loss fraction of up to 59% at higher speeds. This agrees with overall loss trends and previous observations, resulting from higher friction at higher pump

speeds. Electrical losses are showing an inverse trend to the mechanical losses and are dominant in the lower speed region with a loss fraction above 40% for speeds up to 75 rad/s but decreasing towards approximately 28% for the highest speed.

At 148 bar differential pressure, the volumetric loss fraction average increases to 23%, which is 9% higher than for 70 bar, reflecting the pressure dependence of flow loss. The graph shows a slight downward trend for the higher pressure. This is in line with the previously observed trend within the pump of a higher negative speed dependent gradient for higher differential pressures. The mechanical loss fraction scales with speed and reaches a maximum of approximately 33%. The electrical loss fraction remains consistently above 45% for the full speed envelope, being the dominant loss component at 148 bar differential pressure. This is due to the higher pressure requiring a higher torque at the pump shaft, which subsequently leads to a higher motor current. Power loss in electric motors typically scales quadratically with motor current as resistance loss in the windings.

It is evident from these results that the power loss fractions shift both with speed and pressure. The mechanical loss fraction shows a clear speed dependency whereas the electrical and volumetric losses exhibit a pressure dependence. This is most obvious for the electrical losses that become the dominant loss component for 148 bar differential pressure.

The analysis of power loss fractions, enabled by the load cell set-up to determine pump shaft torque allows dominant loss components in different operating modes to be identified. This provides a guide for a detailed breakdown of losses in highly integrated electric pumps, facilitating improved designs.

4.3 Model validation

To support the performance characterization of the pump, the model of Section 2.3 is compared to experimental data. Figure 13 shows a comparison of calculated and measured volumetric and mechanical efficiency (normalized) for three distinct differential pressures across the pump. For commercial reasons, the efficiency results are normalized with respect to the highest respective efficiency value in the data.

To derive a good fit, the analytical model coefficients (see Table 3) were adjusted until a good agreement between model and test results was found.

Table 3: Model coefficients.

Parameter	Value
Slip coefficient $\boldsymbol{c_s}$	$3.5 \cdot 10^{-8}$
Speed coefficient $\boldsymbol{c_\omega}$	$0.55 \cdot 10^{-8}\ \frac{\mathrm{m}^3}{\mathrm{rad}}$
Viscous friction coefficient $\boldsymbol{c_v}$	$5.3 \cdot 10^{4}$
Coulomb friction coefficient $\boldsymbol{c_f}$	0.14
Constant torque $\boldsymbol{T_c}$	0.065 Nm

The model captures the pressure dependence of the volumetric efficiency reasonably well. This is as expected, considering that the main contribution to flow losses in the model is accounted for by the calculation of a total leakage flow, which is inherently pressure dependent. The added speed coefficient proves beneficial to represent the speed dependence of flow losses. In the originally proposed model by Wilson, and later McCandlish and Dorey, the compressibility term is proportional to speed, but negligible in comparison to the leakage loss. Without the speed coefficient, the model therefore assumes nearly constant flow losses with increasing speed – considering that the power output is rising with speed, this leads to higher efficiencies for higher speeds. This indicates that there are speed dependent loss mechanisms present in the tested pump, which need further investigation. Both the speed and pressure dependence of mechanical losses are captured well by the model, indicating that a good set of coefficients was identified.

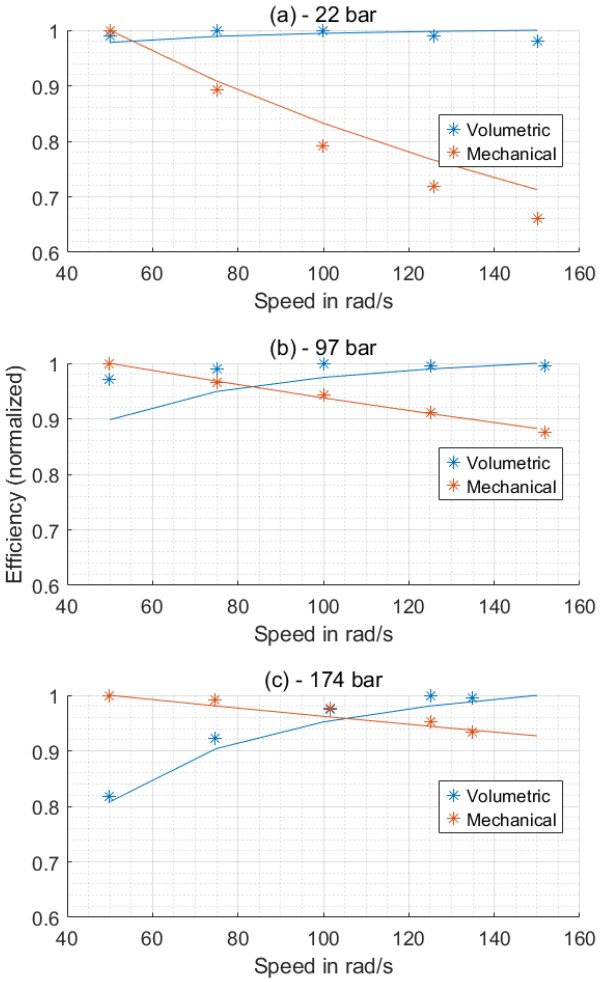

Figure 13: Comparison of experimental (marker) and modelled (line) volumetric and mechanical efficiency (normalized) for (a) 22 bar, (b) 97 bar, and (c) 174 bar differential pressure.

The reasonable agreement between model and test data validates the simplified approach to loss modelling in the pump. The results support common trends in volumetric and mechanical losses within piston type pumps and help identify

regions of high pump operating efficiency. Generally, high pressures are favourable for small mechanical losses, whereas low pressures are preferable for small volumetric losses. Both mechanical and volumetric losses are speed dependent, however this trend is more distinct on the mechanical side due to viscous friction. Overall, the unit under test favours medium speeds and higher pressures as operating conditions as per design intent.

5 Conclusion and outlook

In this study, a novel ePump design and loss analysis framework, including a non-invasive torque measurement approach was presented. This will further enhance the understanding of highly integrated electric pumps. The ePump design is based on a radial piston pump architecture, tightly integrated with a BLDC motor. The design is shaftless, reducing bearing and sealing requirements, and enabling an ultra-compact assembly. The unit not only integrates motor and pump but also features onboard power electronics and closed-loop speed control of the pump with the opportunity of sensing motor temperature for condition monitoring A double lobed cam facilitates 14 piston strokes per revolution, minimizing flow ripple. The loss analysis framework enables the separation of volumetric, mechanical and electrical losses within the unit. Based on this, favourable operating conditions for the respective subsystems can be identified. This will facilitate improved designs for future iterations and allow for design optimizations in terms of size, weight and efficiency.

The proposed torque measurement method was successfully proven. A hysteresis effect was observed in the results with a slight deviation in the torque value between moving up and down a staircase pressure ramp. The measured torque scaled linearly with pressure as expected. Overall, repeatable and credible results could be obtained and enabled the analysis of power loss fractions. This has allowed to identify dominant loss components in different operating modes. The results show that power loss fractions shift both with speed and pressure. The mechanical loss fraction exhibits a clear speed dependency whereas volumetric losses are pressure dependent. The electrical losses demonstrate both pressure and speed dependencies The volumetric loss fraction remains below 30% for all tested operating points. Whilst the mechanical loss fraction reaches up to 59% for the lower pressure setting, mechanical losses stay below 33% for the higher pressure. For the lower pressure, the electrical losses reach up to 61% for the low-speed region but are the overall dominant loss term for the higher pressure operating point with a fraction above 45% for the full speed envelope.

The simple mathematical model was successfully validated and showed reasonable agreement with the experimental data. This validates the simplified approach to loss modelling in the pump. Common piston pump loss trends were observed in the results and high efficiency regions could be identified. Overall, the unit under test favours medium speeds and higher pressures as operating conditions per design intent.

Future work will investigate the hysteresis effect in the torque measurement set up. A more detailed loss model, including physical design parameters such as clearances, piston and cam geometry will be developed and used to improve the understanding of the observed loss mechanisms. Work is ongoing in modelling electric motor losses for a comparison with the measured electrical losses. Additionally, IEC60034-2 will be considered as a framework to break down the electric motor losses. For this study, an early prototype was used as a demonstrator. It is intended to further refine and validate the discussed approach with more units.

Overall, the proposed ePump loss analysis framework was successfully validated with existing hardware and allowed a detailed break-down of losses in the unit under test. This has allowed identification of favourable operating regions and can provide guidance for future design iterations.

References

[1] D. Beltrami, P. Iora, L. Tribioli, and S. Uberti, ‘Electrification of Compact Off-Highway Vehicles—Overview of the Current State of the Art and Trends’, *Energies*, vol. 14, no. 17, p. 5565, Sep. 2021, doi: 10.3390/en14175565.

[2] A. Lajunen, P. Sainio, L. Laurila, J. Pippuri-Mäkeläinen, and K. Tammi, ‘Overview of Powertrain Electrification and Future Scenarios for Non-Road Mobile Machinery’, *Energies*, vol. 11, no. 5, p. 1184, May 2018, doi: 10.3390/en11051184.

[3] D. Li, C. Tan, W. Ge, J. Cui, C. Gu, and X. Chi, ‘Review of Brake-by-Wire System and Control Technology’, *Actuators*, vol. 11, no. 3, p. 80, Mar. 2022, doi: 10.3390/act11030080.

[4] L. Tom, M. Khowja, G. Vakil, and C. Gerada, ‘Commercial Aircraft Electrification—Current State and Future Scope’, *Energies*, vol. 14, no. 24, p. 8381, Dec. 2021, doi: 10.3390/en14248381.

[5] European Commission, ‘COMMUNICATION FROM THE COMMISSION - The European Green Deal’, European Commission, Brussels, Dec. 2019.

[6] S. Ketelsen, D. Padovani, T. Andersen, M. Ebbesen, and L. Schmidt, ‘Classification and Review of Pump-Controlled Differential Cylinder Drives’, *Energies*, vol. 12, no. 7, p. 1293, Apr. 2019, doi: 10.3390/en12071293.

[7] Voith Turbo GmbH & Co KG, ‘Motor/pump hybrid system EPAI for high and medium-pressure applications’. 2012. Accessed: Feb. 23, 2025. [Online]. Available: http://www.hypower.com.hk/pdf/Voith_Turbo/890_e_g1891_en.pdf

[8] W. Wustmann, S. Helduser, U. Schuffenhauer, H. Kuss, and N. Michalke, ‘Fully Integrated Electric-Hydrostatic Drive Based on a Gear Pump And a Switched Reluctance Motor’, in *Proceedings of the Tenth Scandinavian International Conference on Fluid Power, SICFP’07, May 21-23, 2007, Tampere, Finland*, Tampere, Finland, 2007.

[9] F. Zappaterra, A. Vacca, and S. D. Sudhoff, ‘A compact design for an electric driven hydraulic gear machine capable of multiple quadrant operation’, *Mechanism and Machine Theory*, vol. 177, p. 105024, Nov. 2022, doi: 10.1016/j.mechmachtheory.2022.105024.

[10] P. Gamez-Montero *et al.*, ‘GeroMAG: In-House Prototype of an Innovative Sealed, Compact and Non-

Shaft-Driven Gerotor Pump with Magnetically-Driving Outer Rotor', *Energies*, vol. 10, no. 4, p. 435, Mar. 2017, doi: 10.3390/en10040435.

[11] W. Fiebig, D. Ignacy, C. Marek, and K. Hubert, 'A vane pump integrated with an electric motor', in *Proceedings of the 9th International Fluid Power Conference, 9. IFK, March 24-26, 2014, Aachen, Germany*, Aachen, Germany, 2014.

[12] W. Fiebig, P. Cependa, P. Jedraszczyk, and H. Kuczwara, 'Innovative Solution of an Integrated Motor Pump Assembly', in *ASME/BATH 2017 Symposium on Fluid Power and Motion Control*, Sarasota, Forida, USA: American Society of Mechanical Engineers, Oct. 2017, p. V001T01A040. doi: 10.1115/FPMC2017-4277.

[13] M. P. Ciurys and W. Fiebig, 'Experimental Investigation of a Double-Acting Vane Pump with Integrated Electric Drive', *Energies*, vol. 14, no. 18, p. 5949, Sep. 2021, doi: 10.3390/en14185949.

[14] T. Wang and Z. Zhou, 'A Compact Hydrostatic-Driven Electric Generator: Design, Prototype, and Experiment', *IEEE/ASME Trans. Mechatron.*, vol. 21, no. 3, pp. 1612–1619, Jun. 2016, doi: 10.1109/TMECH.2015.2504491.

[15] D. Zhu, Y. Fu, X. Han, and Z. Li, 'Design and experimental verification on characteristics of electro-hydraulic pump', *Mechanical Systems and Signal Processing*, vol. 144, p. 106771, Oct. 2020, doi: 10.1016/j.ymssp.2020.106771.

[16] S. Sarode, L. Shang, A. Vacca, and S. Sudhoff, 'Design methodology for an integrated axial piston-type electrohydraulic unit', *Proceedings of the Institution of Mechanical Engineers, Part C: Journal of Mechanical Engineering Science*, p. 09544062231185517, Jul. 2023, doi: 10.1177/09544062231185517.

[17] E. Lester and M. Miles, 'TwinTorq Electric-Hydraulic Motor.E. Lester, M. Miles'. KersTech, Inc Accelerating Vehicle Technology, Beaverton, Oregon. Accessed: Feb. 23, 2025. [Online]. Available: http://kerstech.com/twintorq/

[18] G. R. Bohach, Nishanth, E. Severson, and J. D. Van De Ven, 'Modeling and Optimization Study of a Tightly Integrated Rotary Electric Motor-Hydraulic Pump', in *ASME/BATH 2019 Symposium on Fluid Power and Motion Control*, Longboat Key, Florida, USA: American Society of Mechanical Engineers, Oct. 2019, p. V001T01A010. doi: 10.1115/FPMC2019-1626.

[19] F. Nishanth, G. Bohach, J. V. De Ven, and E. L. Severson, 'Design of a Highly Integrated Electric-Hydraulic Machine for Electrifying Off-Highway Vehicles', in *2019 IEEE Energy Conversion Congress and Exposition (ECCE)*, Baltimore, MD, USA: IEEE, Sep. 2019, pp. 3983–3990. doi: 10.1109/ECCE.2019.8912685.

[20] F. N. U. Nishanth, G. Bohach, M. M. Nahin, J. Van De Ven, and E. L. Severson, 'Design of an Axial Flux Machine With an Integrated Hydraulic Pump for Off-Highway Vehicle Electrification', in *2020 IEEE Energy Conversion Congress and Exposition (ECCE)*, Detroit, MI, USA: IEEE, Oct. 2020, pp. 1772–1779. doi: 10.1109/ECCE44975.2020.9235731.

[21] F. Nishanth, G. Bohach, M. M. Nahin, J. Van De Ven, and E. L. Severson, 'Development of an Integrated Electro-Hydraulic Machine to Electrify Off-highway Vehicles', *IEEE Trans. on Ind. Applicat.*, vol. 58, no. 5, pp. 6163–6174, Sep. 2022, doi: 10.1109/TIA.2022.3189609.

[22] M. M. Nahin, G. R. Bohach, F. N. U. Nishanth, E. L. Severson, and J. D. Van De Ven, 'Dynamic Modeling and Design of a Radial Hydrostatic Piston Pump for Integrated Pump-Motor', in *ASME/BATH 2021 Symposium on Fluid Power and Motion Control*, Virtual, Online: American Society of Mechanical Engineers, Oct. 2021, p. V001T01A028. doi: 10.1115/FPMC2021-68788.

[23] J. Li, X. Meng, P. Dong, and S. Zhao, 'Design and analysis of an axial flux permanent magnet motor for the direct drive radial piston pump', *Proceedings of the Institution of Mechanical Engineers, Part C: Journal of Mechanical Engineering Science*, vol. 233, no. 19–20, pp. 7077–7088, Oct. 2019, doi: 10.1177/0954406219869970.

[24] A. Plummer, 'Integrated Hydromechatronic Actuators', in *2023 IEEE International Conference on Mechatronics (ICM)*, Loughborough, United Kingdom: IEEE, Mar. 2023, pp. 1–6. doi: 10.1109/ICM54990.2023.10101880.

[25] *BS ISO 4409:2019 - Hydraulic fluid power — Positive displacement pumps, motors and integral transmissions — Methods of testing and presenting basic steady state performance*, 2019.

[26] P. Achten *et al.*, 'Measuring the Losses of Hydrostatic Pumps and Motors: A Critical Review of ISO4409:2007', in *ASME/BATH 2019 Symposium on Fluid Power and Motion Control*, Longboat Key, Florida, USA: American Society of Mechanical Engineers, Oct. 2019, p. V001T01A007. doi: 10.1115/FPMC2019-1615.

[27] C. Schänzle and P. F. Pelz, 'Meaningful and Physically Consistent Efficiency Definition for Positive Displacement Pumps - Continuation of the Critical Review of ISO 4391 and ISO 4409', in *ASME/BATH 2021 Symposium on Fluid Power and Motion Control*, Virtual, Online: American Society of Mechanical Engineers, Oct. 2021, p. V001T01A027. doi: 10.1115/FPMC2021-68739.

[28] *BS ISO 8426:2008 - Hydraulic fluid power — Positive displacement pumps and motors — Determination of derived capacity*, 2008.

[29] W. E. Wilson, 'Rotary-Pump Theory', *Journal of Fluids Engineering*, vol. 68, no. 4, pp. 371–384, May 1946, doi: 10.1115/1.4018484.

[30] D. McCandlish and R. E. Dorey, 'The Mathematical Modelling of Hydrostatic Pumps and Motors', *Proceedings of the Institution of Mechanical Engineers, Part B: Management and engineering manufacture*, vol. 198, no. 3, pp. 165–174, Aug. 1984, doi: 10.1243/PIME_PROC_1984_198_062_02.